

Smart Cement Characterization Based on Laboratory and Field Test Data Using Artificial Intelligent (AI) Models with Vipulanandan Models for Application in Cemented Wells and Micropiles

C. Vipulanandan Ph.D., P.E.

“Smart Cement” Inventor

“Vipulanandan Rheological Model”

“Vipulanandan Failure Model”

Chief Editor – Advances in Civil Engineering

Director, Center for Innovative Grouting Material and Technology (CIGMAT)

Director, Texas Hurricane Center for Innovative Technology (THC-IT)

Professor of Civil and Environmental Engineering

University of Houston, Houston, Texas 77204-4003

Abstract

Recently smart cement, highly sensing chemo-thermo-piezoresistive cement has been developed with a real-time monitoring system for applications in cemented wells and all types of civil infrastructures including micropiles. The smart cement is a bulk sensor and there are no sensors buried in it. In this study, laboratory and field test data were used to verify the Artificial Intelligent (AI) models with Vipulanandan models for smart cement applications. The performance of the smart cement in the cemented wells will be very much influenced by the hydration of the cement which is affected by the environment and ground geological conditions. Hence laboratory tests were performed to collect the data for AI model training and verification and also set the baseline for comparing it with the cement hydration in the field test model simulating the cemented wells and micropiles. Electrical resistivity, a material property, has been selected to monitor the smart cement from the time of mixing to the entire service life. The resistivity changed by over 12.85 times (1285%) in 28 days under the room curing condition, indicating the sensitivity of resistivity for monitoring. Smart cement is piezoresistive cement and the piezoresistivity strain at compressive stress failure for the smart cement was over 250% , over 1250 times (125,000%) higher than the compressive failure strain of 0.2%. The field well was installed using standard casing of $9\frac{5}{8}$ inches (245 mm) in diameter and was cemented using the smart cement with enhanced piezoresistive properties. The field well was designed, built, and used to demonstrate the concept of real time monitoring of the flow of smart cement and hardening of the cement in place. The well was installed in soft swelling clay soils to investigate the sensitivity of the smart oil well cement. A new method has been developed to measure the electrical resistivity of the materials in the laboratory and field using the two probe method. The well instrumentation was outside the casing with 120 probes, 18 strain gages and 9 thermocouples. The strain gages and thermocouples were used to compare the sensitivity of these instruments to the two probe resistance measure in-situ in the cement. The electric probes used to measure the resistance were placed vertically at 15 levels and each level had eight horizontal probes. Change in the resistance of hardening cement was

continuously monitored since the installation of the field well for over 4.5 years (1600 days) and over 10,000 data have been collected. Also, the temperature and strain changes in the cement were measured at various depths. The field well cement performances were very much influenced by the weather changes and the depth in the ground and the resistivity change varied by 270% to 950% based on the depth of the cement sheath. In addition, the pressure testing showed the piezoresistive response of the hardened smart cement and a piezoresistive model has been developed to predict the pressure in the casing from the change in resistivity in the smart cement.

Both laboratory and field data including weather data were used in this analyses. Total of over 1500 data were used in this study and 80% of the data were used for training the AI model and 20% of the data were used to verify the AI model predictions with Vipulanandan model prediction. Initially various AI models with multiple layers of artificial neural networks were first calibrated using the generalized regression neural network (GRNN) and back propagation neural network (BPNN) and then evaluated for the predictions of the remaining 20% of the test data. The predicted evaluation was done using the statistical parameters such as coefficient of determination (R^2) and root mean square error (RMSE). The four layer artificial neural network AI model was selected for predicting the experimental results. The AI model didn't predict the initial curing of the smart cement well, since resistivity reduced to a minimum value and then continuously increased. The AI models predicted the long-term laboratory smart cement curing and piezoresistive behavior and field data of resistivity changes with depth and time very well and were comparable to the Vipulanandan p-q curing and piezoresistivity model behavior models. Based on the coefficient of determination (R^2) and root mean square error (RMSE), Vipulanandan models predicted the experimental results very well. Also the AI model predicted the temperature and annual rainfall weather changes over the 4.5 years very well.

1. Introduction

With the advancement of various technologies, there is a need to integrate them for more efficient field applications for real-time monitoring, minimizing failures and safety issues. Use of artificial intelligent (AI) in various applications with multiple variables are becoming popular. Cementing the oil wells have been used for over 200 years cementing failures during installation and other stages of operations have been clearly identified as some of the safety issues that have resulted in various types of delays in the cementing operations and oil production and also has been the cause for some of the major disasters around the world. For successful oil well cementing operations, it is essential to monitor it real-time because of the varying environmental and geological conditions with depth and also performance of the cement sheath after hardening during the entire service life.

Artificial Intelligence (AI), otherwise known as machine learning or computational intelligence, is the science and engineering aimed at creating intelligent tools, devices and machines. Its application in solving complex problems and case-based complications in various field applications has become more and more popular and

acceptable over time (Opeyemi et al., 2016). AI techniques are developed and deployed worldwide in a myriad of applications as a result of its symbolic reasoning, explanation capabilities, potential and flexibility (Demrigan et al. 2011). Most of the artificial intelligence techniques or tools have shown tremendous potential for generating accurate analysis and results from large historical databases, the kind of data an individual may find extremely difficult for conventional modelling and analysis processes (Shahab 2000). AI is currently employed in various sections of oil and gas Industry, from selection of drill bits to well bore risk analysis. In recent years, there has been a drastic increase in the application of AI in petroleum industry due to presence of digital data and case studies. AI can provide real time prediction in oil and gas industry from selection, monitoring, diagnosing, predicting and optimizing, thus leading to better production efficiency and profitability. (Opeyemi et al., 2016)

Wells (Oil, Gas and Water)

Well construction has a history of over 100 years. When installing oil, gas and water production wells, cement is used to fill the annular space between varying geological formations with depth and well casings and horizontal pipelines to enhance the performance in-situ for decades after installation. Based on the application, wells can be tens to thousands of feet deep in the ground. The cement will support the casing and pipelines and protect them against corrosion and impact loading, restrict the movement of fluids between formations, and isolate productive and nonproductive zones. Well cement is used under different conditions of exposures compared to the cement used in the conventional construction industry. The strength of well cement usually depends on factors such as time and conditions of curing, environmental conditions, slurry design and use of additives and any additional treatments to the cement. Different additives have been used in the cement to mitigate the strength degradation (Choolaei et al. 2012). The real-time monitoring of the changes in the cement in-situ is critical to evaluate the performance of the cemented wells (Vipulanandan et al. 2015-2018). Recent case studies on cementing failures have clearly identified several issues that resulted in various types of delays in the cementing operations. Also preventing the loss of fluids to the formations and proper well cementing have become critical issues in well construction to ensure wellbore integrity because of varying downhole conditions (Labibzadeh et al., 2010 and Vipulanandan et al., 2015). The catastrophic accident in the Gulf of Mexico in April 2010 is one of the world's worst oil spills (Shadravan et al., 2012). Therefore, proper monitoring and tracking the entire process of well cementing become important to ensure cement integrity during the service life of the well (Vipulanandan et al., 2015-2018).

Micropiles

The use of micropiles has grown significantly since their conception development in the 1950s. Micropiles are generally used when there are difficult ground conditions, such as natural or man-made obstructions, sensitive ground with adjacent structures, limited access/low headroom and/or karstic geology. They are commonly used to replace deteriorating foundation systems, for the renovation of structures, to support structures affected by adjacent construction, for seismic retrofitting or in-situ reinforcement including embankment, slope and landslide stabilization.

Micropile configuration includes a steel casing and/or high strength steel reinforcements bonded to the bearing soil or rock with the cement grout. Micropile is a non-displacement pile with the typical diameter of 5 to 12 inches over 200 feet in length to carry loads of over 200 tons. Uniqueness about the micropile is that it can be install at any angle based on the applications.

Smart cement (sensing cement)

Based on the applications, Portland cements and well cement were mixed with less than 0.1% conductive filler (carbon fibers, basaltic fiber or a mixture with diameter in the micrometer range) to make the cement chemo-thermo-piezoresistive material (Vipulanandan et al., 2014-2018). Smart cement can sense any changes going on inside the borehole during cementing and during curing after the cementing job. The smart cement can sense the changes in the water cement ratio, different additives, and any pressure applied to the cement sheath in terms of piezoresistivity (Vipulanandan et al. 2015). Recent studies have demonstrated that smart cement can also detect gas leaks and also earthquakes. The failure compressive strain for the smart cement was 0.2% at peak compressive stress (Vipulanandan et al. 2015b) and the resistivity change is of the order of two hundred percent (200%) making it over 1000 times more sensitive.

Artificial Intelligent (AI)

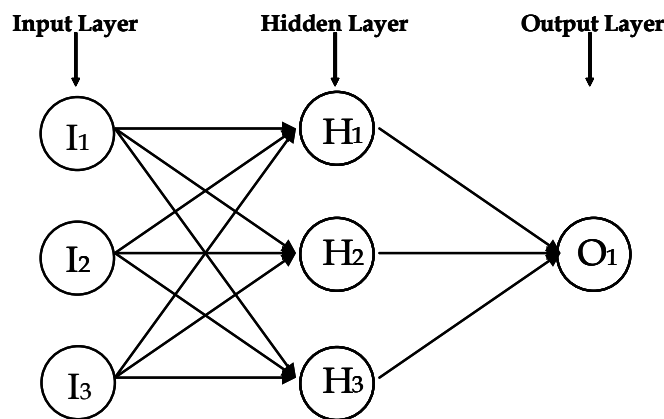


Figure 1. Artificial Intelligent (AI) with Integrated Artificial Neural Networks (ANN)

An artificial neural network (ANN) is a computational numerical model which is

based on, at some level, brain like learning as opposed to traditional computing which is based on programming. The model consists of interconnected groups of artificial neurons, which simulate the structure of the brain to store and use experience, and processes information using a connectionist approach. Artificial neural network is an adaptive system which trains itself (changes its structure) during the learning phase based on the information flowing through the network.

The researchers who have studied neural networks aimed to model the fundamental cell of the living brain: neuron. The recognized US pioneers who first introduced the concept of artificial neural network were neurophysiologist Warren McCulloch and the logician Walter Pitts in 1943. They developed a simple model of variable resistors and summing amplifiers that represent the variable synaptic connections or weights which link neurons together and the operation of the neuron body, respectively. The popularity of neural network increased in 1962 with the introduction of ‘perceptron’ by Frank Rosenblatt who used the term to refer to a system which recognized images using the McCulloch and Pitts model (Alexander 1990).

Artificial Intelligence (AI) can be defined as a collection of new analytical algorithms and tools that attempts to imitate and predict situations. These Artificial intelligence techniques exhibit an ability to learn and deal with new situations. Artificial neural networks, evolutionary programming and fuzzy logic are among the paradigms that are classified as Artificial Intelligence (Sadiq et al., 2000). The main root principles of AI include reasoning, knowledge, planning, learning, communication, perception and ability to manipulate objects (Bhattacharyya, 2011).

Artificial Neural Networks (ANN)

Neural Network research was first published by McCulloch and Pitts in 1943 (Hubbert et al., 1957). The artificial neural network is a numerical model that mimics the functional aspects of neural network in human brain system (Behnood et al., 2018). It consists of many artificial neurons interconnected where each of them gives a single output (Y) induced from all inputs (X_i) (Hammoudi et al., 2019). The predictive capability of artificial neural networks comes from the ability to learn and adapt to new situations in which additional data becomes available. In an artificial neural network, a training set comprising of input and output data is entered and the neural network algorithms attempt to map the process by which inputs become outputs (Sadiq et al., 2000). ANN is a multilayer perceptron (MLP) including three layers (Fig. 1). The first layer (input layer) consists of neurons representing the independent variables (inputs X_i), the second one is the hidden layer (H_i, f(H_i)), and the last one is the ANN responses (output layer, representing AI). The number of neurons required in the hidden layer is determined in a way to minimize both prediction error and number of neurons.

The general forms of the equations are as follows:

$$H_j = \sum W_{ij}X_i + b_j \dots\dots\dots(1)$$

Where X_i represent the inputs (Fig. 1, neurons I) and subscript i represents the inputs (I and summation 1 to n). The W_{ij} is the weighing matrix for each input term X_i connecting it to the hidden term H_j, The b_j is the bias input function.

Using Sigmoid as the transfer function $f(H_j)$ is represented as

$$f(H_j) = 1 / (1 + e^{-H_j}) \dots\dots\dots (2)$$

Two accurate neural network algorithms are Back Propagation Neural Networks (BPNN) and Generalized Regression Neural Networks (GRNN). The following are the summaries on these algorithms.

Back Propagation Neural Networks (BPNN)

BPNN are the most widely used type of artificial neural networks (Sadiq et al., 2000). BPNN consists of an input layer that is propagated through the network with set of weights to have a predicted output. BPNN is set with an objective to adjust the set of weights so that the difference between output prediction and required output is reduced.

Generalized Regression Neural Networks (GRNN)

The generalized regression neural network (GRNN) is a feedforward neural network based on non-linear regression theory consisting of three or more layers: the input layer (one layer), the pattern layer with the summation layer (one or more layers), and the output layer. While the neurons in the first three layers are fully connected, each output neurons is connected only to some processing units in the summation layer. The individual pattern units compute their activation using a radial basis function (bj), which is typically the Gaussian kernel function (Sadiq et al., 2000). The training of the GRNN is quite different from the training used for the BPNN. It is completed after presentation of each input-output vector pair from the training set to the GRNN input layer only once. What this means is that both the centers of the radial basis functions of the pattern units and the weights in connections of the pattern units and the processing units in the summation layer are assigned simultaneously.

Development of Neural Network and Design

The data used in this study were obtained from set of laboratory and field scale studies on smart cement. The obtained data comprises of electrical resistance, piezoresistive strain data from lab for 28 days and field for a period of 4.5 years. Database preparation for training of neural network represents very important in neural network modelling. The suggested neural network model does not consider weather and temperature factors. Neural network architecture with different hidden layers was used to predict laboratory and field measurements. Attempts were made to use hidden layers from one to four to obtain a good fit to the data. BPNN architecture with 4 hidden layers exhibited better correlation to laboratory and field measurements. The coefficient of determination (R^2) and root mean-square-error (RMSE) were used to evaluate the statistical significance of the ANN models.

Smart Cement

Cement is the largest quantity of material manufactured in the world, 4.2 trillion tons in 2017, and is used in many applications. Chemo-thermo-piezoresistive smart cement has been recently developed (Vipulanandan et al. 2014-2017) which can sense and real-time monitor the many changes happening inside the cement during cementing of wells

to concreting of various infrastructure to the entire service life of the structures. In concrete smart cement is the binder which can sense the changes within the concrete. The smart cement can sense the changes in the water-to-cement ratios, different additives, contamination and pressure applied to the cement sheath or concrete in terms of chemo-thermo-piezoresistivity. The failure compressive strain for the smart cement was 0.2% at peak compressive stress and the resistivity change is of the order of several hundred percentage making it over 500 times (50,000%) more sensitive (Vipulanandan et al. 2014-2017).

2. Objective

The smart cement behavior must be quantified during various stages of construction and service life of the cemented well. In this study the smart cement behavior was characterized using artificial intelligent models and compared to the Vipulanandan models to verify the predictions of the experimental results. The specific objectives were as follows:

- i. Investigate the available AI tools for potential applications based on the selected data trends.
- ii. Characterize the curing and piezoresistive behavior of smart cement from laboratory test data using the selected AI model and compare it to the Vipulanandan models.
- iii. Compare the AI predictions of changes in the hardening smart cement sheath resistivity over 4.5 years along the smart cemented field well with multiple variables (ground conditions, depths, time, and weather) with the available analytical models.
- iv. Predict the sensitivity of the piezoresistive response of the hardened smart cement sheath using the AI and analytical model.

The data for this study was collected from the laboratory tests and field test and total of over 1,500 data was used.

3. Materials and Methods

Smart cement is a chemo-thermo-piezoresistive material and the changes in the directional electrical properties were monitored during the testing to quantify the changes. Both class G and class H cements were used in this study. The electrical resistivity is a second order tensor so the changes can be interpreted in three orthogonal directions to monitor the changes in the smart cement. Series of experiments were performed on the smart cement from the time of mixing to hardened state behavior using a new characterization approach with the two-probes and alternative current to monitor changes in electrical properties. This real time monitoring method can be easily adopted in the field. Effects of contamination and temperature on the directional properties were investigated. Also compressive tests were performed to monitor the changes in the smart cement cured under various conditions. Various types and levels of AI models are being used to predict the behaviors and comparing them to some of the analytical models.

Total of four wires were placed in the mold and the vertical distances between any two wires were the same. Embedment depth of the conductive wire was 1 inch. For setting time monitoring and compressive stress tests, cylinders with the diameter of 50

mm (2 inches) and a height of 100 mm (4 inches) were prepared. For real-time monitoring, a two-probe method was selected (Vipulanandan et al. 2013 & 2017). In this study, three or more specimens were prepared and tested under every condition investigated and the data were used in the analyses.

Electrical resistivity

Digital resistivity meter was used to measure the resistivity of the cement slurries and semi-solids. The measurable resistivity range for the instrument was 0.01Ω-m to 400 Ω-m. The device was calibrated using standard solutions of sodium chloride (NaCl). The electrical resistance was measured using an inductance, capacitance, and resistance (LCR) meter during the cement curing and compression/pressure test in the laboratory and field. To minimize the contact resistances, the resistance was measured at 300 kHz using the two-wire method. The electrical resistivity (ρ) was related to the measured electrical resistance (R) based on the Eqn.1 (Vipulanandan et al. 2013 & 2017).

$$\rho = \frac{R}{K + GR} \dots\dots\dots(3)$$

where parameters K and G are related to the material being tested and method used. For cement experimentally it has been proven that the parameter G is zero. Hence the normalized change in resistivity with the changing conditions (curing, stress) can be represented as follows:

$$\frac{\Delta\rho}{\rho} = \frac{\Delta R}{R} \dots\dots\dots(4)$$

In this study resistivity (ρ) was used for all monitoring changes in the laboratory and field.

Piezoresistivity test

The cylindrical specimen with the diameter of 2 inches and a height of 4 inches (50mm Dia.*100 mm height) was capped (sulfur capping) and tested at a predetermined controlled displacement rate. Compression tests were performed on cement samples after 28 days of curing using a hydraulic compression testing machine (ASTM C 39). Piezoresistivity describes the change in the electrical resistivity of a material under pressure. Since oil well cement serves as the pressure-bearing part of wells in real applications, the piezoresistivity of smart cement was investigated under compressive loading. During compression testing, electrical resistance was measured along the stress axis and laterally. To eliminate the polarization effect, alternating current resistance measurements were made using a LCR meter at a frequency of 300 kHz (Vipulanandan et al. 2013).

In this study chemo-thermo-piezoresistive smart cement (Vipulanandan et al. 2014-2018) was used to develop the concrete and grout. For the curing and compressive behavior studies cement slurry was cast in plastic cylindrical molds with diameter of 50 mm and a height of 100 mm. Two conductive wires were placed in all of the molds to

measure the changing in electrical resistivity. At least three specimens were tested under each condition investigated in this study.

Compression Test (ASTM C39)

The cylindrical specimens (concrete, cement and grout) were capped and tested at a predetermined controlled displacement rate. Tests were performed in the Tinius Olsun machine at a controlling the displacement rate to 0.125 mm per minute. In order to measure the strain, a commercially available extensometer (accuracy of 0.001% strain) was used. During the compression test, the change in resistance was measured continuously using the LCR meter. Two probe method with alternative current (AC) at 300 kHz frequency was used in order to minimize the contact resistances (Vipulanandan and Amani, 2015). The change in resistance was monitored using the two-probe method, and the parameter in Eqn. (2) was used relate the changes in resistivity to the applied stress.

4. Results and Analyses

During curing the electrical properties of the smart cement varied with the curing conditions in the laboratory and field. New quantification concepts have been developed using artificial intelligent models to characterize the sensing of the smart cement during curing and during loading to quantify the piezoresistive behavior in the laboratory and field.

Laboratory Study

Curing of cement

Initial resistivity was measured immediately after mixing the smart cement. Initial resistivity of the smart cement was 1.05 Ωm (Table 1). During the curing process under room condition (relative humidity of 50% and temperature of 72°F (22°C)), the resistivity rapidly changed with the time as shown in Fig. 2. Hence, there are several parameters that can be used in monitoring the curing (hardening process) of the cement. The parameters are initial resistivity (ρ_o), minimum resistivity (ρ_{\min}), time to reach the minimum resistivity (t_{\min}) and resistivity after 24 hours of curing (ρ_{24}). After initial mixing, the electrical resistivity reduced to a minimum value (ρ_{\min}), and then it gradually increased with time. Time to reach minimum resistivity, t_{\min} , can be used as an index of speed of chemical reactions and cement set times. With the formation of resistive solid hydration products which block the conduction path, resistivity increased sharply with curing time. The following increase in electrical resistivity was caused by the formation of large amounts of hydration products in the cement matrix. Finally, a relatively stable increase in trend was reached by the ions diffusion control of hydration process, and resistivity increased steadily with the curing time.

Table 1: Electrical Resistivity Model parameters for smart cement in laboratory for 28 days of curing.

Cement Type	Initial Resistivity, ρ_0 (Ω -m)	ρ_{min} (Ω -m)	t_{min} (min)	t_0 (min)	R^2	p_1	q_1
Smart Cement	1.05 ± 0.03	0.96 ± 0.01	80 ± 5.0	110	0.99	0.61	0.38

Vipulanandan p-q curing model

Based on experimental results, a theoretical model proposed by Vipulanandan and Paul (1990) was modified and used to predict the electrical resistivity of smart cement during hydration. The Vipulanandan p-q curing model (Vipulanandan et al. 2015) is defined as follows:

$$\frac{1}{\rho} = \left(\frac{1}{\rho_{min}}\right) \left(\frac{\left(\frac{t+t_0}{t_{min}+t_0}\right)}{q_1 + (1-p_1-q_1) \left(\frac{t+t_0}{t_{min}+t_0}\right) + p_1 \left(\frac{t+t_0}{t_{min}+t_0}\right)^{p_1}} \right)^{\frac{p_1+q_1}{p_1}} \dots\dots\dots(5)$$

Where ρ is the electrical resistivity (Ω -m); t is the curing time (minutes); ρ_{min} : minimum electrical resistivity (Ω -m); t_{min} : time corresponding minimum electrical resistivity (ρ_{min}), $p_1(t)$, t_0 and $q_1(t)$ are model parameters. In general, model parameters are influenced by the composition of the cement and curing conditions (temperature, humidity and stress). The parameter t_0 is influenced by the initial resistivity ρ_0 .

0.5 Day Curing

The normal trend of the resistivity during the curing of cement is that the resistivity decreases up to a certain time (t_{min}) to reach the minimum resistivity (ρ_{min}) and then increases with time. The value of initial resistivity of smart cement was 1.05Ω .m. immediately after mixing, which can be used as a quality control measure in the field. The value of minimum resistivity was 0.96Ω .m. and the time for minimum resistivity was 80 minutes after mixing (Figure 2). The resistivity after 0.5 day (12 hours) of curing was 2.27Ω .m, more than doubled in resistivity compared to the initial resistivity. The resistivity after 12 hours (0.5 day) was over 116% compared to the initial resistivity.

For training the AI models with one, two, three and four layers of ANN, total of 120 data were used with the GRNN approach. Based on the training results, four layer AI model was selected to do the predictions. Additional 30 data was used to predict the smart cement curing trend using the AI model and compare it to the Vipulanandan Curing Model. In predicting the new data, for the four layered AI model the coefficient of determination (R^2) was 0.61 and the RMSE (root mean square error) was 0.21Ω .m. The AI model prediction is compared to the experimental data in Fig. 2. The AI model over predicted the initial resistivity by 3% and also couldn't predict the minimum resistivity.

Vipulanandan Model parameters p_1 and q_1 were 0.61 and 0.38 (Table 1). This model predicted the curing trend very well including the minimum resistivity (Fig. 2). The coefficient of determination (R^2) was 0.98 and the RMSE (root mean square error) was 0.05Ω .m (Table 2).

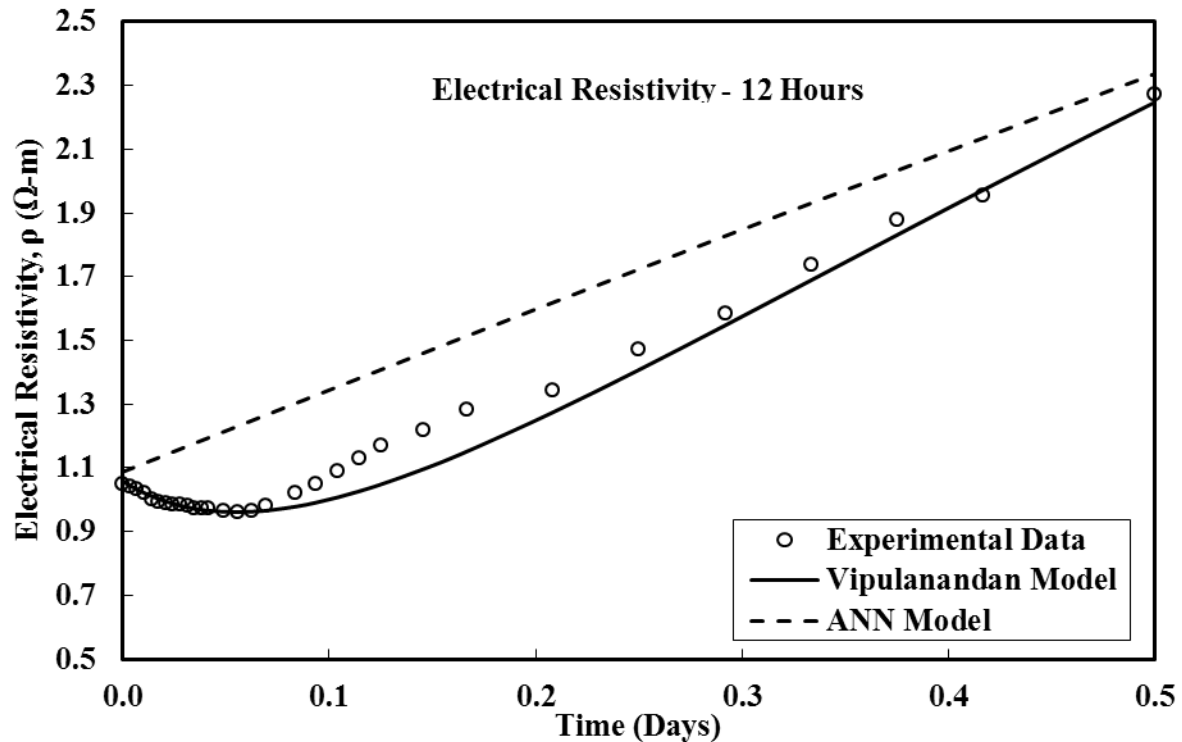


Figure 2. Electrical Resistivity of Smart Cement in the Laboratory During 0.5 Day of Curing.

1 Day Curing

The resistivity after 1 day (24 hours) of curing was 3.46 $\Omega\cdot\text{m}$, more than 230% increase compared to the initial resistivity. The resistivity after 24 hours (1 day) was over 50% higher compared to the resistivity after 12 hours (0.5 day).

For training the AI models with one, two, three and four layers of ANN, total of 160 data were used with the GRNN approach. Based on the training results, four layer AI model was selected to do the predictions. Additional 40 data was used to predict the smart cement curing trend using the AI model and compare it to the Vipulanandan Curing Model. In predicting the new data, for the four layered AI model the coefficient of determination (R^2) was 0.92 and the RMSE (root mean square error) was 0.19 $\Omega\cdot\text{m}$. The AI model prediction is compared to the experimental data in Fig. 3. The AI model predicted the 24 hour resistivity very well.

Vipulanandan Model parameters p_1 and q_1 were 0.61 and 0.38 (Table 1). This model predicted the curing trend very well including the minimum resistivity (Fig. 3). The coefficient of determination (R^2) was 0.99 and the RMSE (root mean square error) was 0.08 $\Omega\cdot\text{m}$ (Table 2).

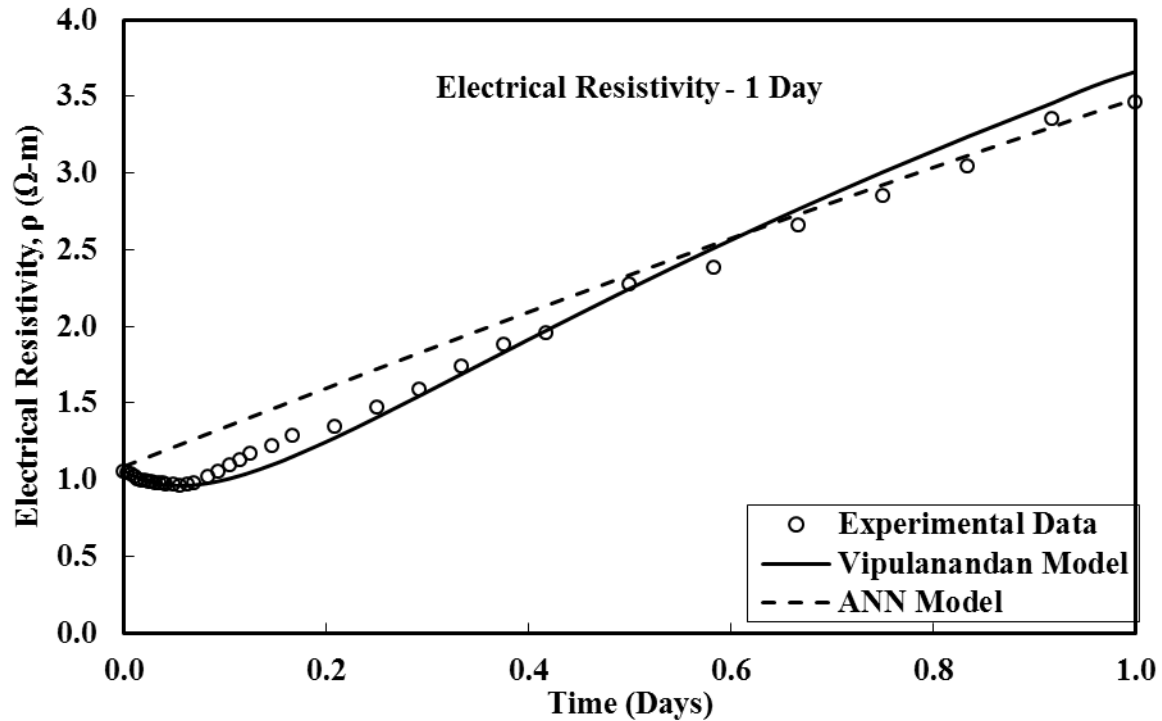


Figure 3. Electrical Resistivity of Smart Cement in the Laboratory During 1 Day of Curing.

28 Days of Curing

The resistivity after 28 days of curing was 14.54 $\Omega\cdot\text{m}$, more than 1285% increase compared to the initial resistivity. The resistivity after 28 days of curing was over 320% higher compared to the resistivity after 24 hours (1 day). This clearly indicates the sensitivity of resistivity to the cement curing.

For training the AI models with one, two, three and four layers of ANN, total of 180 data were used with the GRNN approach. Based on the training results, four layer AI model was selected to do the predictions. Additional 45 data was used to predict the smart cement curing trend using the AI model and compare it to the Vipulanandan Curing Model. In predicting the new data, for the four layered AI model the coefficient of determination (R^2) was 0.99 and the RMSE (root mean square error) was 0.20 $\Omega\cdot\text{m}$. The AI model prediction is compared to the experimental data in Fig. 4. The AI model predicted the 28 days of curing resistivity very well .

Vipulanandan Model parameters p_1 and q_1 were 0.61 and 0.38 (Table 1). This model also predicted the curing trend very well (Fig. 4). The coefficient of determination (R^2) was 0.99 and the RMSE (root mean square error) was 0.21 $\Omega\cdot\text{m}$ (Table 2).

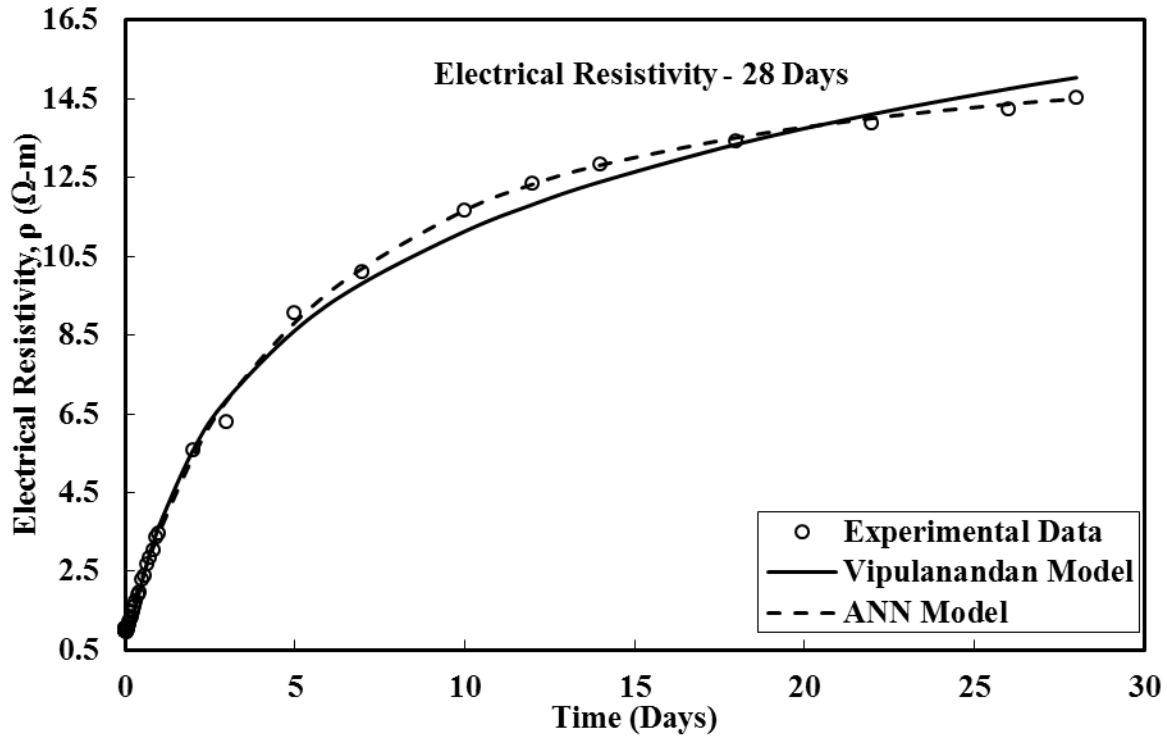


Figure 4. Electrical Resistivity of Smart Cement in the Laboratory During 28 Days of Curing.

Table 2: Comparison of ANN Model and Vipulanandan Resistivity Model Predictions for Curing of Smart Cement.

Time	ANN Model		Curing Model	
	R ²	RMSE (Ω-m)	R ²	RMSE (Ω-m)
T = 12 hours	0.61	0.21	0.98	0.05
T = 1 Day	0.92	0.19	0.99	0.08
T = 28 Days	0.99	0.20	0.99	0.21

Piezoresistivity Behavior

It is important to characterize the sensing property, resistivity change, of the smart cement under stress. The piezoresistive responses (stress-resistivity strain relationship) for the smart cement is shown in Fig. 5 for 28 days cured smart cement. The piezoresistivity of the smart cement at failure after 28 day of curing $\left(\frac{\Delta\rho}{\rho_0}\right)_f$ was 252% as shown in Fig. 5. The smart cement piezoresistive response was over 1250 times (125,000%) higher compared to the compressive failure strain of cement of 0.2%, which is used in the past for monitoring. This also clearly indicates the sensitivity of smart cement for stress monitoring in the cement.

Vipulanandan p-q piezoresistivity model

The Vipulanandan p-q piezoresistivity model was used to predict the observed

trends for the smart cement (Vipulanandan et al. 2014). The Vipulanandan p-q piezoresistive model is defined as follows:

$$\sigma = \frac{\sigma_{max} \times \left(\frac{\left(\frac{\Delta\rho}{\rho} \right)}{\left(\frac{\Delta\rho}{\rho} \right)_0} \right)}{q_2 + (1 - p_2 - q_2) \times \left(\frac{\left(\frac{\Delta\rho}{\rho} \right)}{\left(\frac{\Delta\rho}{\rho} \right)_0} \right) + p_2 \times \left(\frac{\left(\frac{\Delta\rho}{\rho} \right)}{\left(\frac{\Delta\rho}{\rho} \right)_0} \right)^{\left(\frac{p_2 + q_2}{p_2} \right)} \dots\dots\dots(6)$$

where σ is the stress (psi or MPa); σ_f : compressive stress at failure (MPa); $x = \left(\frac{\Delta\rho}{\rho_0} \right) * 100$ is percentage of change in electrical resistivity due to the stress; $x_f = \left(\frac{\Delta\rho}{\rho_0} \right)_f * 100$ is the percentage of change in electrical resistivity at failure; $\Delta\rho$: change in electrical resistivity; ρ_0 : initial electrical resistivity ($\sigma = 0$ MPa) and p_2 and q_2 are piezoresistive model parameters.

28 Days of Curing

It is important to quantify the piezoresistive behavior of the smart cement. The specimens were cured under room condition and the stress- piezoresistive strain response was non-linear (Figure 5).

For training the AI models with one, two, three and four layers of ANN, total of 80 data were used with the GRNN approach. Based on the training results, four layer AI model was selected to do the predictions. Additional 20 data was used to predict the smart cement piezoresistive behavior using the AI model and compare it to the Vipulanandan piezoresistive Model. In predicting the new data, for the four layered AI model the coefficient of determination (R^2) was 0.99 and the RMSE (root mean square error) was 0.20 MPa. The AI model prediction is compared to the experimental data in Fig. 5.

Vipulanandan Model parameters p_2 and q_2 were 0.108 and 0.57 (Table 1). This model also predicted piezoresistive behavior very well (Fig. 5). The coefficient of determination (R^2) was 0.99 and the RMSE (root mean square error) was 0.24 MPa (Table 3). Both the AI model and Vipulanandan Piezoresistive Models predicted the behavior very well.

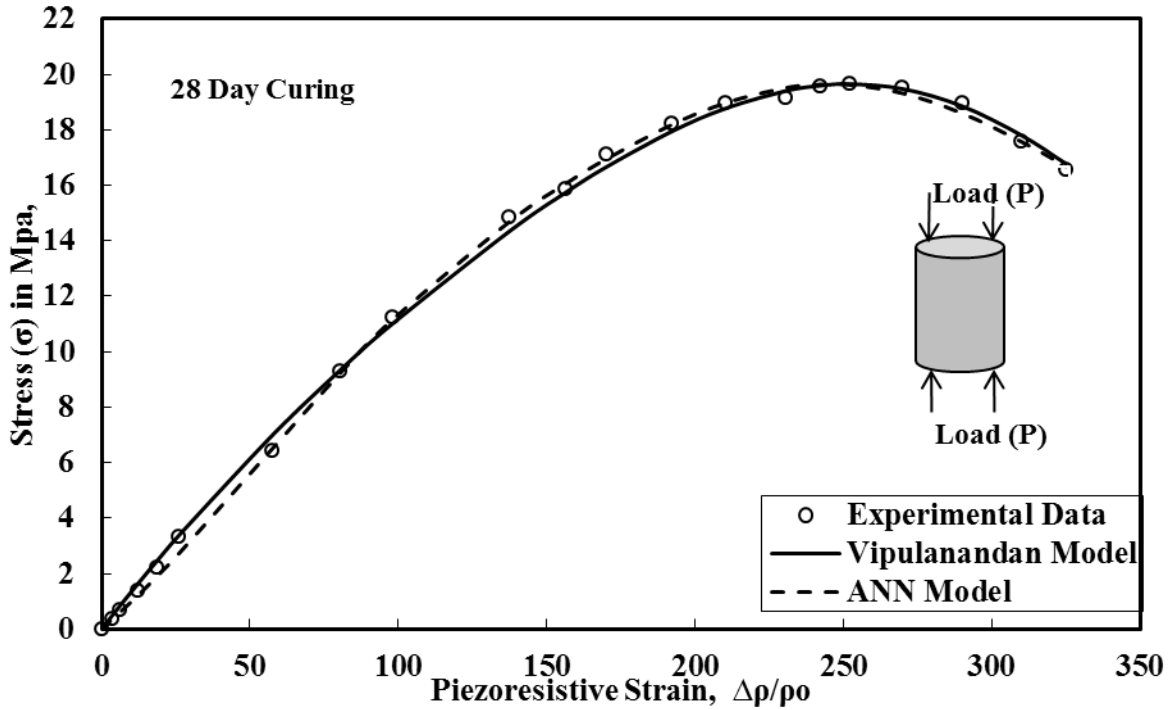


Figure 5: Piezoresistive Behavior of Smart Cement after 28 days of curing.

Table 3: Correlation parameters for ANN model and Piezoresistivity model for smart cement after 28 days of curing.

Time	ANN Model		Piezoresistive Model	
	R ²	RMSE (MPa)	R ²	RMSE (MPa)
28 Day Piezoresistivity	0.99	0.20	0.99	0.24

Field Study

After reviewing a few potential test sites, Energy Research Park (ERP) at the University of Houston, Houston Texas was selected to install the field well. Many factors including geology, swelling and soft clays, changing surrounding conditions (weather, ground water and active zone in the ground), environmental regulations and accessibility to the site for long-term monitoring had to be considered in selecting the test site since the focus of the study was to demonstrate the sensitivity of the smart cemented field well. The selected site had swelling clays with fluctuating moisture conditions (active zone) which represents the nearly the worst conditions that could be encountered when installing oil wells. The top 20 feet of the soil was swelling clay soil with liquid limit of over 50%. Based on ASTM classification, this soil was characterized as CH soil. The active zone in the Houston area is about 15 feet, indicating relatively large moisture fluctuation in the soil causing it to swell and shrink. The water table was 20 feet below ground and soil below the water table was also clay with less potential for swelling and the liquid limit was below 40%. Based on ASTM classification, this soil was

characterized as CL soil.

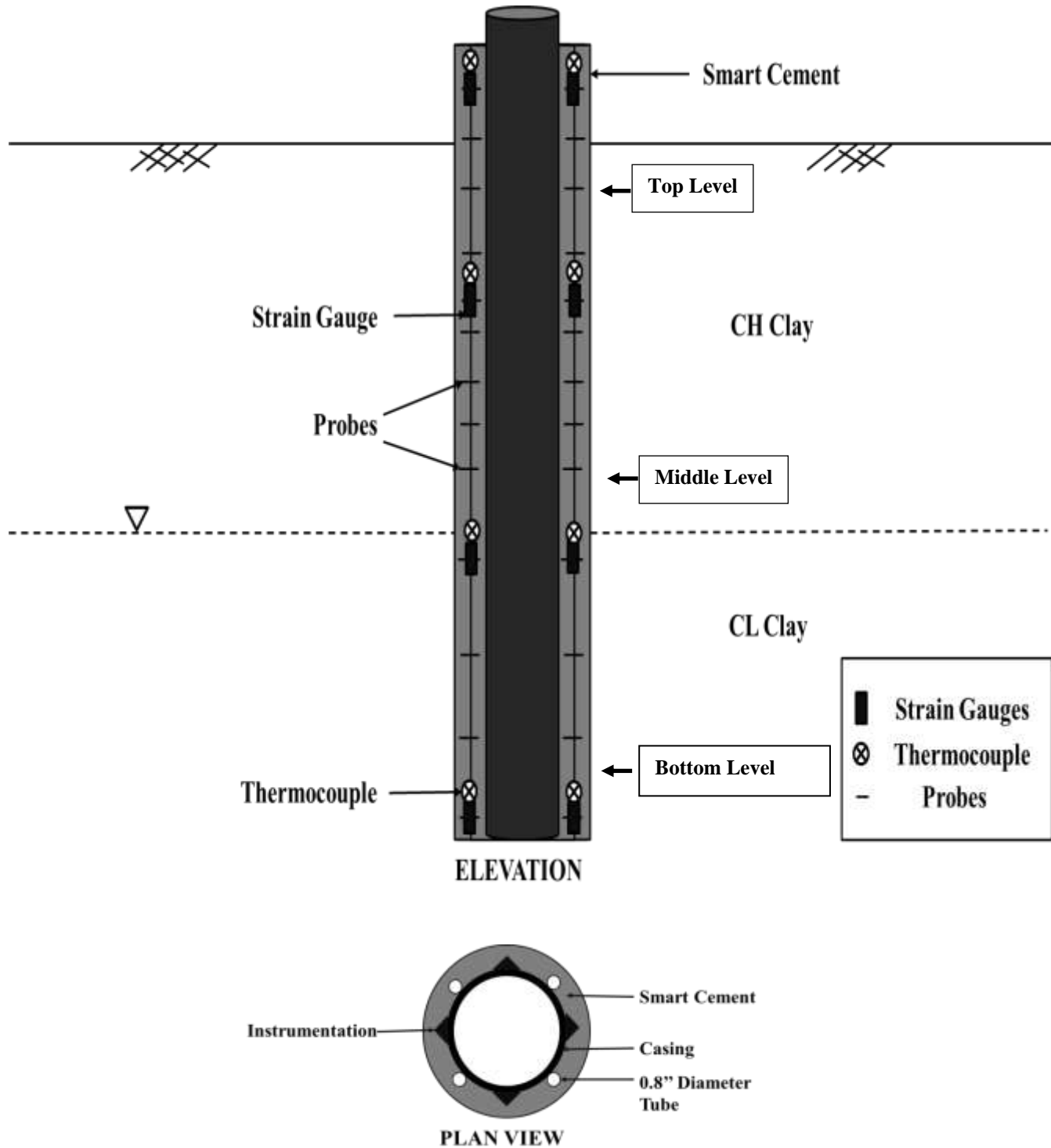


Figure 6 Schematic View of the Field Well with the Instrumentation

Instrumentation

It has been shown that the two probes with AC current can be used to determine the electrical resistance changes in the smart cement and drilling fluid (Vipulanandan 2015 (a)-(d)). It was also important use other standard tools for measuring the changes in the cement sheath and compare it to the resistance changes. Because of practical reasons no instrument was placed on the casing and totally an independent system was developed to be place in the cement sheath. The probes were placed at various vertical depths at 15 levels (Fig. 6). Also eight probes were placed horizontally at each level. Also nine stain gages and nine thermocouples were included in the instrumentation (Fig. 6).

Installation of the Field Well

A commercial company familiar with the drilling and cementing wells in an urban setting was selected to install the field well. A very large drilling truck with drilling with 14 in diameter drill was used to drill the hole and place the 9⁵/₈ in diameter standard steel casing. The total length of the casing was 42 feet and needed pieces (including well head and needed connections to lift the casing) were welded together to make a single unit. Initial 15 feet was drilled without any drilling fluid. Polymer based drilling fluid was used to drill the rest of the borehole. After completing the drilling the casing and the instrumentation units were centered and lowered into the borehole. Monitoring of the resistance between the probes, temperature and stains (straing gages) were measured.

Pressure Test

To simulate a pressure test, air pressure (P_i) was applied inside the 0.8 in diameter tube to the entire depth of 40 feet (Fig. 15) to verify the piezoresistivity of the cement-sheath. Initially the electrical resistances (R_o in Ohms) were measured along the entire depth before applying the pressure. This test was done regularly to demonstrate the sensitivity of the smart cement to the applied small pressures of up to 80 psi (0.55 MPa).

Environmental Factors – (Temperature and Rainfall)

The behavior of smart cement in the field was affected by the outside environmental factors such as temperature, rainfall, stress, water table and swelling soft clay. In this study ANN model was compared with the Temperature model and cumulative rainfall model to predict the changes in temperature and rainfall over the past five years from 2015 to 2019.

Temperature

The average monthly atmospheric temperature fluctuated between 85 °F to 48 °F from 2015 to 2020 (Fig. 7).

Vipulanandan Temperature Model

The Vipulanandan temperature model was used to predict the average monthly temperature with time:

$$y - y_o = A * Sin(B(t - t_o)) \dots\dots\dots (7)$$

Where: A and B are model parameters, y_o= initial correction factor for average

temperature, and
 t_0 = initial correction factor for the time.

For training the AI models with one, two, three and four layers of ANN, total of 60 data were used with the BPNN approach. Based on the training results, four-layer AI model was selected to do the predictions. AI model was compared it to the Vipulanandan temperature Model. In predicting the temperature data, using the four-layered AI model the coefficient of determination (R^2) was 0.94 and the RMSE (root mean square error) was 2.75°F. The AI model prediction is compared to the experimental data in Fig. 7.

Vipulanandan Temperature Model parameters A, B, t_0 and y_0 are 15.4°F, 1, 71.1 year and 2.09°F respectively. The coefficient of determination (R^2) was 0.91 and the RMSE (root mean square error) was 3.48°F (Table 4). Both the AI model and Vipulanandan Temperature Models predicted the temperatures well (Fig.7).

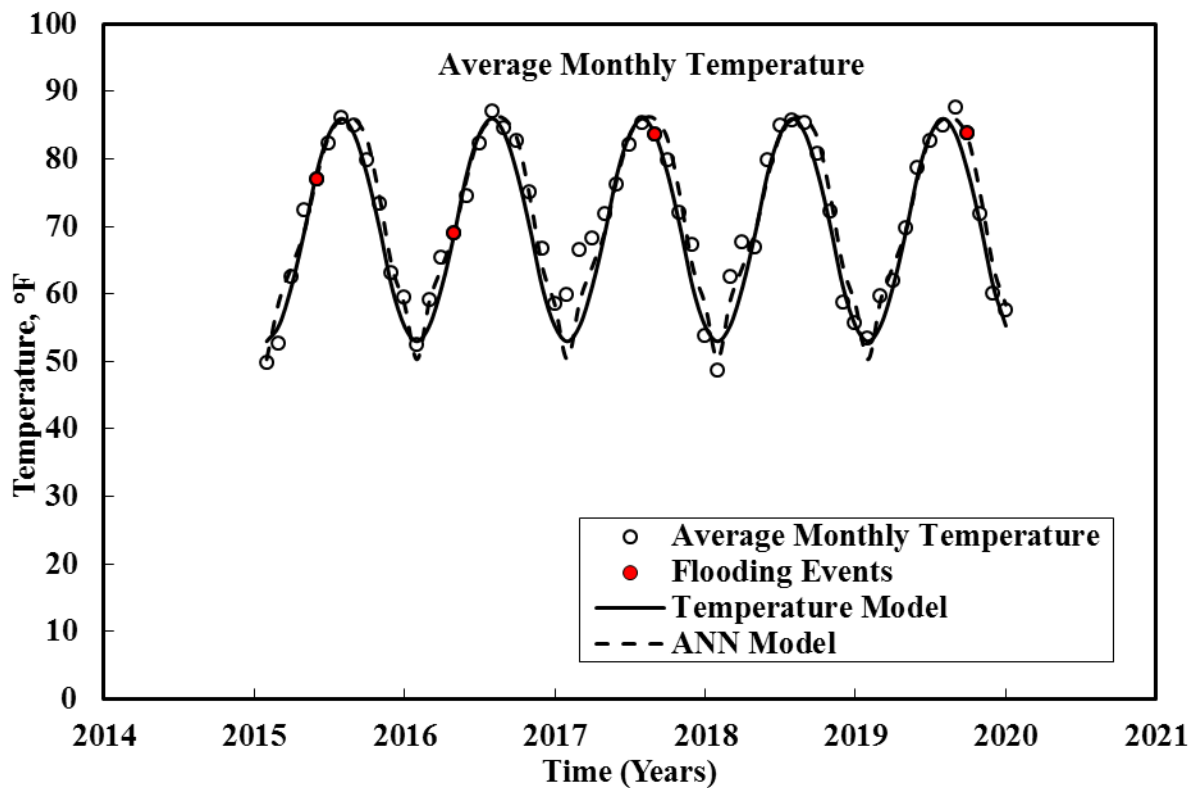


Figure 7 Comparing the Average Monthly Temperature from Year 2015 to 2020 with the Model Predictions.

Rainfall

The cumulative annual rainfall varied from 51 to 80 inches from 2015 to 2020. The four flooding events during this period as shown in Fig. 7 (years 2015, 2016, 2017 and 2019).

Vipulanandan Rainfall Model

The mathematical model was used to predict the cumulative annual rainfall (RF) is using the Vipulanandan Correlation Model (Vipulanandan et al. 1995-2018) is as follows:

$$RF = \frac{t}{C+D*t} \dots\dots\dots(8)$$

Where the parameters C and D are model parameters and t is the month starting from January (equal to 1) to December (equal to 12).

For training the AI models with one, two, three and four layers of ANN, total of 60 data were used with the BPNN approach. Based on the training results, four-layer AI model was selected to do the predictions. AI model was compared it to the Vipulanandan Rainfall Model. In predicting the temperature data, using the four-layered AI model the coefficient of determination (R^2) was 0.86 and the RMSE (root mean square error) was 9.22 inches. The AI model prediction is compared to the experimental data in Fig. 8.

Vipulanandan Rainfall Model parameters C and D are 0.24 (month/inch) and -5.2×10^{-3} /inch respectively. The coefficient of determination (R^2) was 0.74 and the RMSE (root mean square error) was 9.29 inches (Table 4). Both the AI model and Vipulanandan Rainfall Model predicted are compared with the data in Fig.8.

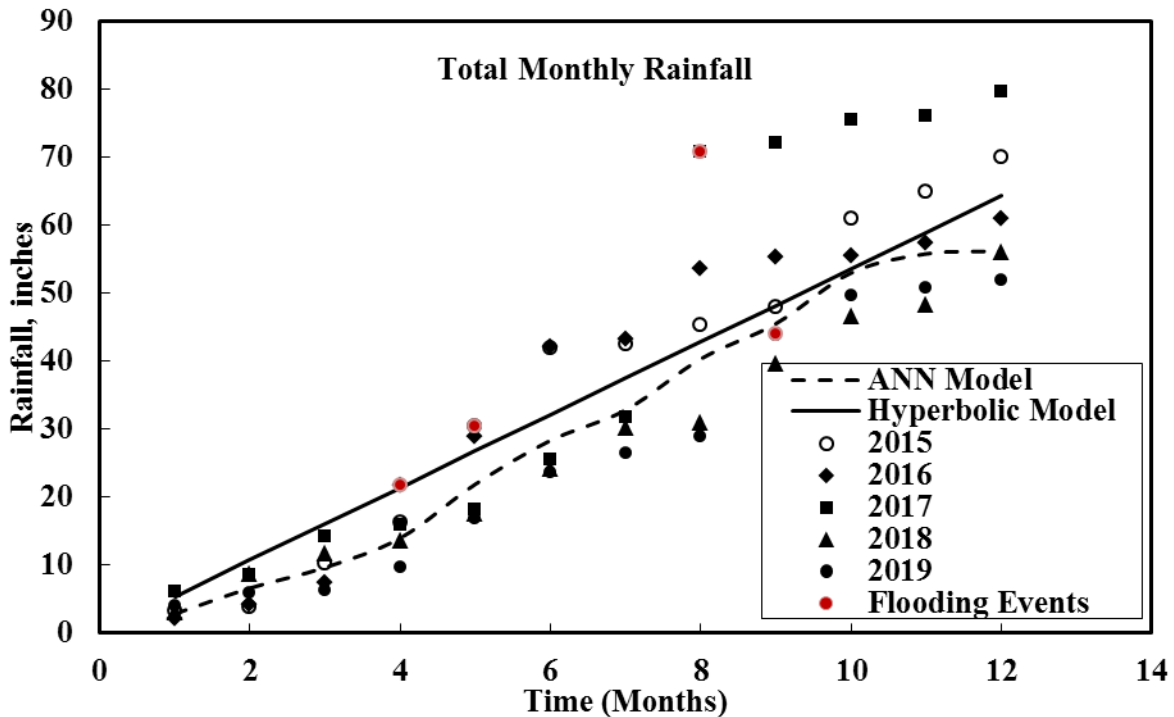


Figure 8 Comparing the Cumulative Monthly Rainfall Predictions from 2015 to 2020

Table 4: Model correlation parameters for temperature and rainfall

Parameter	ANN Model		Temperature/Rainfall Model	
	R ²	RMSE	R ²	RMSE
Temperature	0.94	2.75	0.91	3.48
Rainfall	0.86	9.22	0.74	9.29

Monitoring of Resistance, Strain and Temperature

The smart cement was mixed in the field and used for cementing the field well. It is important to identify the measureable parameters in the cement sheath and also determine the changes with time and depth. Fiber optics are used for monitoring and it depends in the changes in the strain in the cement sheath. The strain in the cement will be influenced by the cement curing, stress and temperature in the cement sheath. Over the past 4.5 years (over 1600 days) thousands of data has been collected on the monitoring parameters. It is important to quantify the changes in the measuring parameters with important variable such as depth. In order to investigate the changes with depth, top level (CH soil), middle level (above the water table, CH soil) and the bottom level (below the water table, CL soil) were selected for investigation.

Top Level

Resistance (R): The top level was about 1 ft. below the ground surface. The initial resistivity of the smart cement measured using the two probes was 1.03 Ω .m comparable to the laboratory mixed cement of 1.05 Ω .m. The resistance in the top level changed from 22 Ω to 221 Ω , about 9.05 times (905%) change in the resistance (Figure 9). The changes in the cement sheath resistance were not uniform but overall showed continuous increase. The rapid increase in the cement resistance was due to the lowering of the environmental temperature and losing of moisture in the cement. The rapid decrease in the cement resistance was due to increase in the environmental temperature and saturation of the cement due to flooding.

Temperature (T): The temperature continuously fluctuated with time with no clear trend. Over the 4.5 years the minimum and maximum measured temperature in the cement sheath was 68°F (20.1°C) and 97.2°F(36.2°C), maximum change of 42.8% (Fig. 9). The average temperature at the top level was about 77.7°F (25.4 °C), a 14% decrease from initial temperature of 90.3°F (32.4°C) which would have been influenced by cement hydration.

Strain (S): The strain gage resistance increased from 123 Ω to 133 Ω during the period of 4.5 years with some fluctuations. The change in strain gage resistance was about 8.1%. The tensile strain at the top level was about 3.3xE-6.

Based on the measured monitoring parameters in the cement sheath, change in electrical resistance showed the largest change compared to the changes in temperature and strain. Hence it is important to develop models to predict this change with time for monitoring the well.

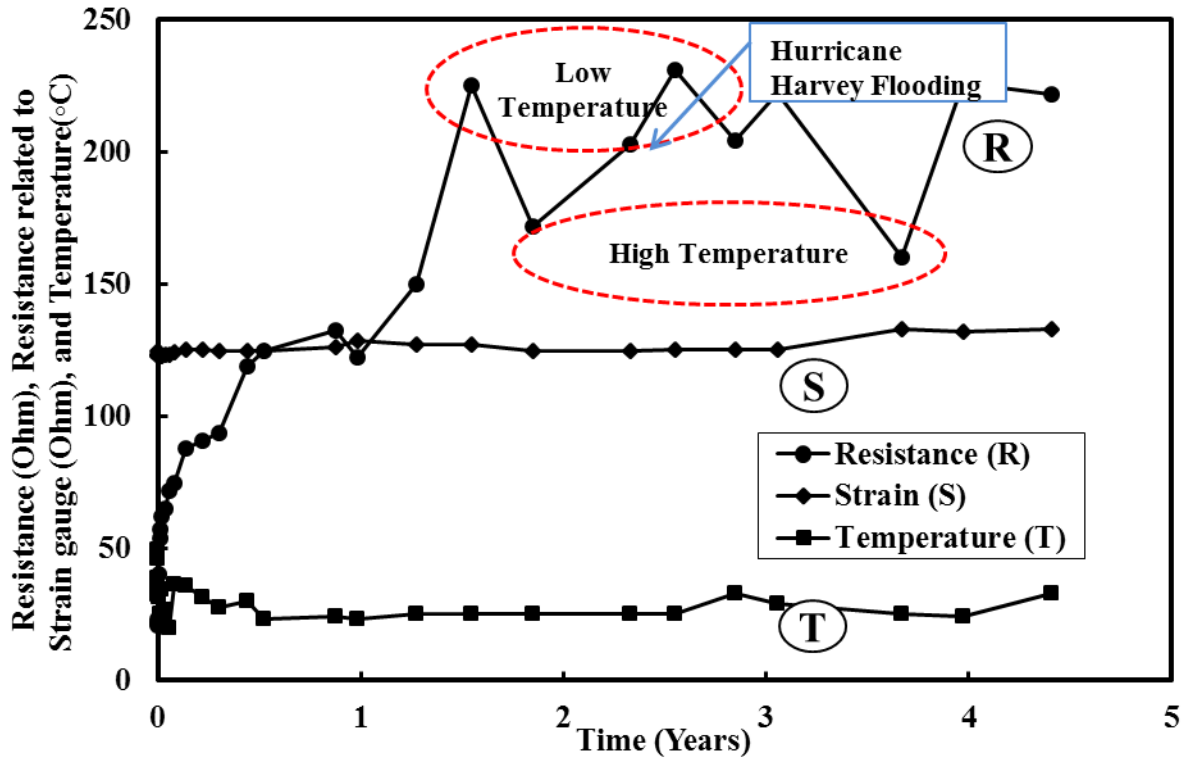


Figure 9: Electrical Resistance, Strain and Temperature variation in top level after 4.5 years.

Middle Level

Resistance (R): The middle level was about 15 ft. below the ground level and above the water table. The initial resistivity of the smart cement measured using the two probes was 1.24 Ω .m higher than top level of 1.03 Ω .m and the laboratory mixed cement of 1.05 Ω .m. The resistance in the top level changed from 26.5 Ω to 182.9 Ω , about 5.90 times (590%) change in the resistance (Figure 10). The changes in the cement sheath resistance were not uniform but overall showed continuous increase. The rapid increase in the cement resistance was due to the lowering of the environmental temperature and losing of moisture in the cement. The rapid decrease in the cement resistance was due to increase in the environmental temperature and saturation of the cement due to rising of the water table because of flooding.

Temperature (T): The temperature continuously fluctuated with time with no clear trend. Over the 4.5 years the minimum and maximum measured temperature in the cement sheath was 70.9°F (21.6°C) and 95.5°F(34.7°C), maximum change of 34.7% (Fig. 10). The average temperature at the middle level was about 78.8°F (26 °C), a 18% decrease from initial temperature of 96.4°F (35.8°C) which would have been influenced by cement hydration.

Strain (S): The strain gage resistance increased from 124 Ω to 132 Ω during the period

of 4.5 years with some fluctuations. The change in strain gage resistance was about 6.5%. The tensile strain in the middle level was 3.65×10^{-6} .

Based on the measured monitoring parameters in the cement sheath, change in electrical resistance showed the largest change compared to the changes in temperature and strain. Hence it is important to develop models to predict this change with time for monitoring the well.

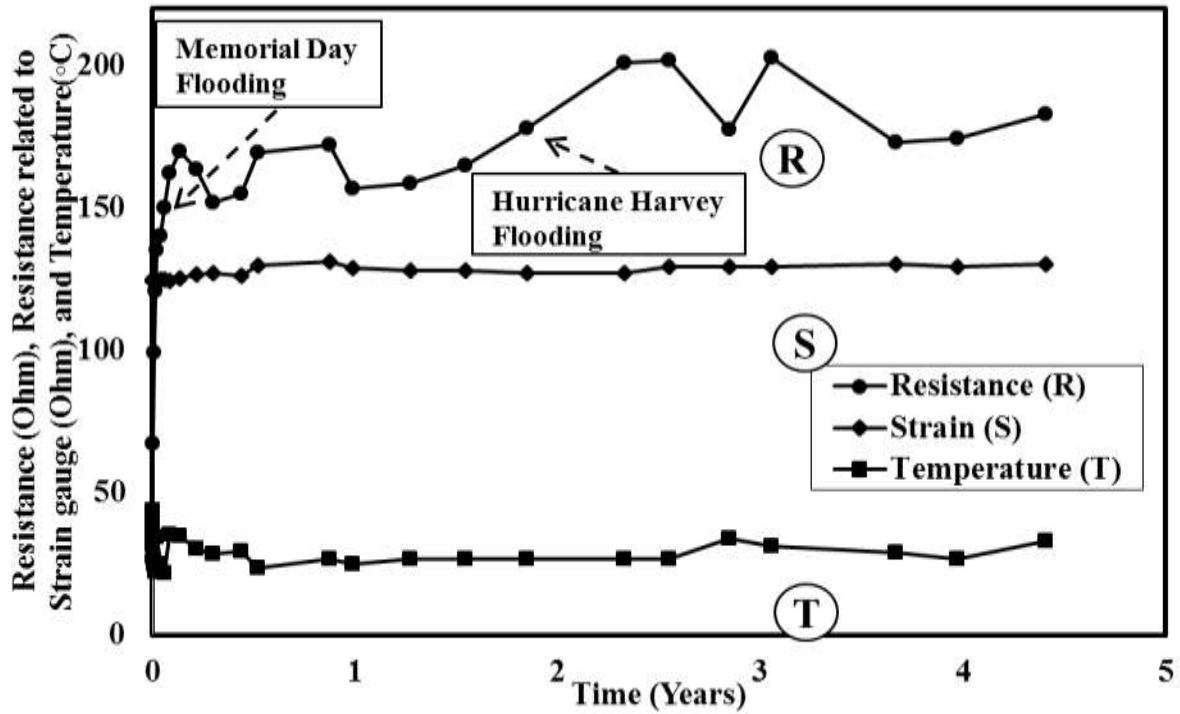


Figure 10: Electrical Resistance, Strain and Temperature variation in middle level after 4.5 years.

Bottom Level

Resistance (R): The bottom level was at 36 ft. below the ground and was under the water table.

The initial resistivity of the smart cement measured using the two probes was $1.32 \Omega \cdot m$ higher than top level of $1.03 \Omega \cdot m$ and the laboratory mixed cement of $1.05 \Omega \cdot m$. The resistance in the bottom level changed from 28.2Ω to 104.9Ω , about 2.72 times (272%) change in the resistance (Figure 11). The changes in the cement sheath resistances were uniform and overall showed continuous increase. The minor fluctuations are due to changes in water table level due to flooding.

Temperature (T): The temperature fluctuated with time but was much less than the middle and top levels. Over the 4.5 years the minimum and maximum measured temperature in the cement sheath was $71.1^\circ F (21.7^\circ C)$ and $91.4^\circ F (33^\circ C)$, maximum

change of 28.6% (Fig. 11). The average temperature at the bottom level was about 77°F (25°C), a 15.8% decrease from initial temperature of 91.4°F (33°C) which would have been influenced by cement hydration.

Strain (S): The strain gage resistance increased from 124 Ω to 133 Ω during the period of 4.5 years with some fluctuations. The change in strain gage resistance was about 8.6%. The tensile strain at the bottom level was 4.8x10⁻⁶.

Based on the measured monitoring parameters in the cement sheath, change in electrical resistance showed the largest change compared to the changes in temperature and strain. Hence it is important to develop models to predict this change with time for monitoring the well.

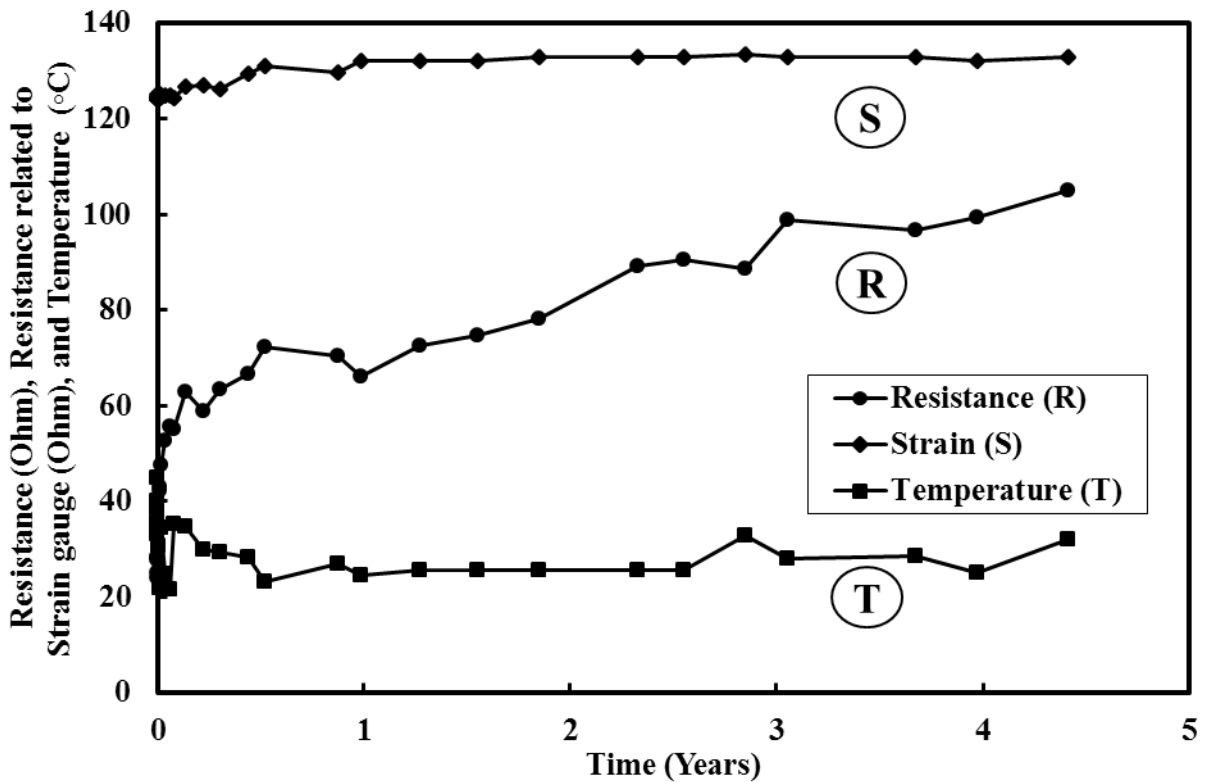


Figure 11 Electrical Resistance, Strain and Temperature variation in bottom level after 4.5 years.

Comparing Resistance Change

From the measurements made at all levels, clearly the electrical resistance change was the highest. Hence it is of interest compare the changes and trends in the electrical resistance with the depth. The electrical resistance change was not uniform in the top and middle levels in the field well. The electrical resistance changed by 905% in the top level close to the surface. The top level also showed the largest fluctuation in the resistance changes based on the weather patters. Both the environmental temperature and rainfall influenced the fluctuation in the resistance at the top level (Fig. 12) The electrical resistance changed by 590% in middle level (15 feet below the ground) with much less

in fluctuation compare to the top level. The electrical resistance change at the bottom level, below the water table, was 272% (Fig. 12). Also the difference in the electrical resistance changes was due to difference in cement curing conditions of the field well. The top level was exposed to outside temperature and had air curing, while the middle level was under moisture curing and bottom level was cured under water.

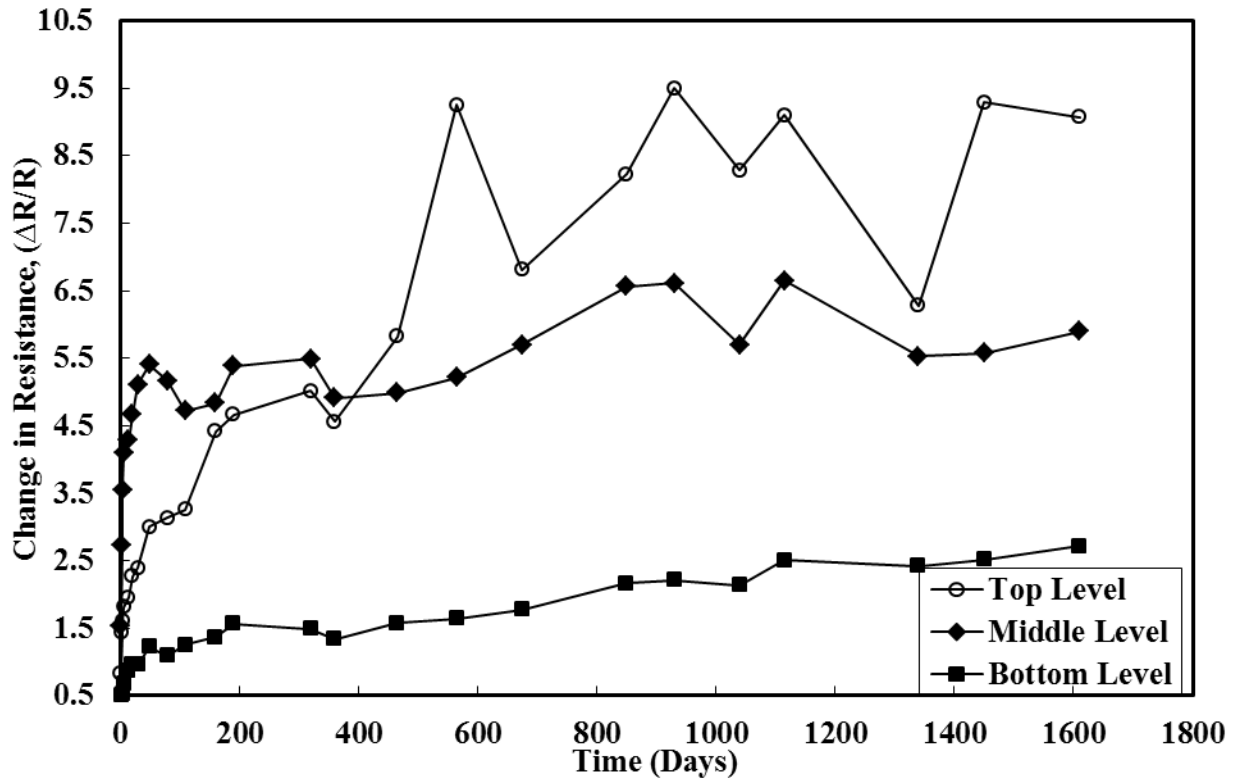


Figure 12. Electrical Resistance data for top, middle and bottom levels in field well for 4.5 years.

Prediction of Electrical Resistivity of Smart Cement

Top Level

The value of initial resistivity of smart cement was 1.03 Ω.m. immediately after mixing. The electrical resistivity of smart cement was 10.4 Ω.m. after 4.5 years of curing (Figure 13). The time for minimum resistivity was 195 minutes after mixing (Table 5). Based on the preliminary analyses, AI model with for layers of ANN was selected predict the resistivity change with time. Over 30 data was used perform the BPNN and also predict the experimental trend. Curing Model parameters p_1 and q_1 were 0.76 and 0.24 respectively after 4.5 years of curing (Table 5). Also the other curing model parameters are summarized in Table 5. The value of RMSE (root mean square error) for curing model was 0.86 Ω.m, while it was 1.02 Ω.m for the AI model. The value of R^2 for curing model was 0.97 while it was 0.91 for the AI model (Table 6). Thus, Vipulanandan curing

model had comparatively better prediction for long term compared to AI model.

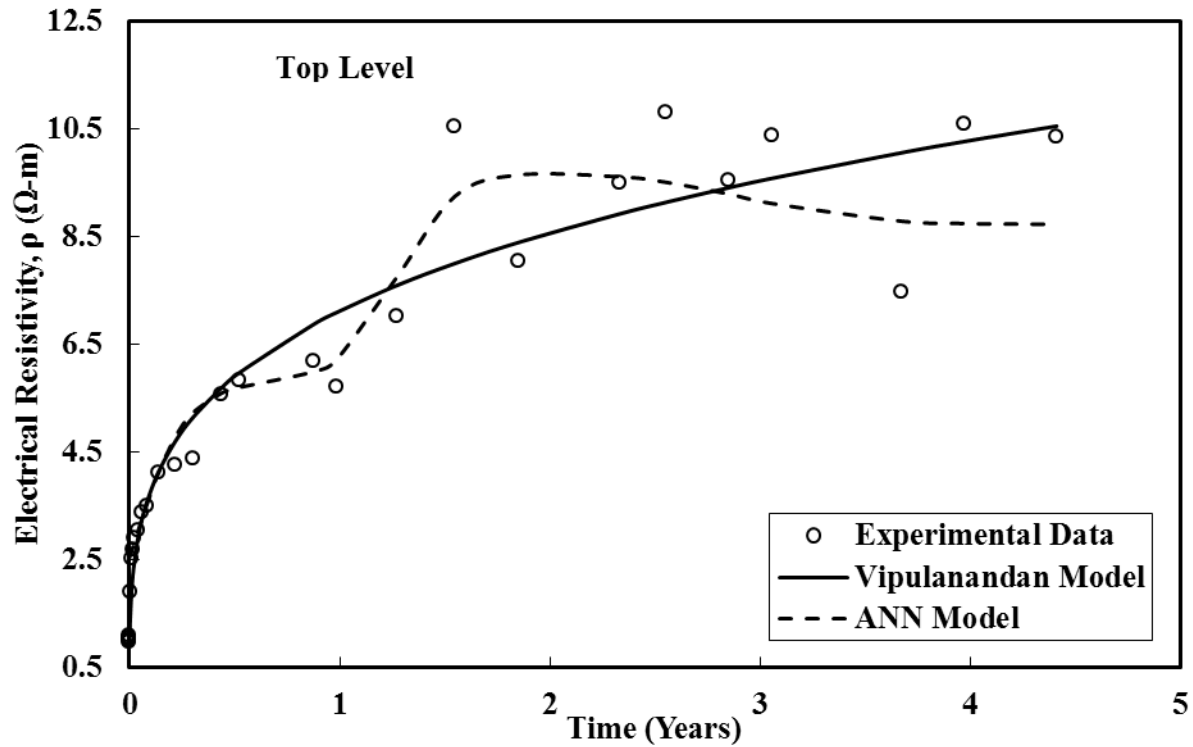


Figure 13. Comparing the Prediction of Electrical Resistivity at the Top Level Using the AI Model and Vipulanandan Curing Model up to 4.5 years.

Middle Level

The value of initial resistivity of smart cement was 1.24 Ω.m. immediately after mixing. The electrical resistivity of smart cement was 8.5 Ω.m. after 4.5 years of curing (Figure 14). The time for minimum resistivity was 195 minutes after mixing (Table 5). Based on the preliminary analyses, AI model with for layers of ANN was selected predict the resistivity change with time. Over 30 data was used perform the BPNN and also predict the experimental trend. Curing Model parameters p_1 and q_1 were 0.78 and 0.22 respectively after 4.5 years of curing (Table 5). Also the other curing model parameters are summarized in Table 5. The value of RMSE (root mean square error) for electrical resistivity model was 1.44 Ω.m while it was 1.73 Ω.m for AI model. The value of R^2 for electrical resistivity model was 0.91 while it was 0.61 for AI model (Table 6). Thus, Vipulanandan curing model had comparatively better prediction for long term compared to AI model.

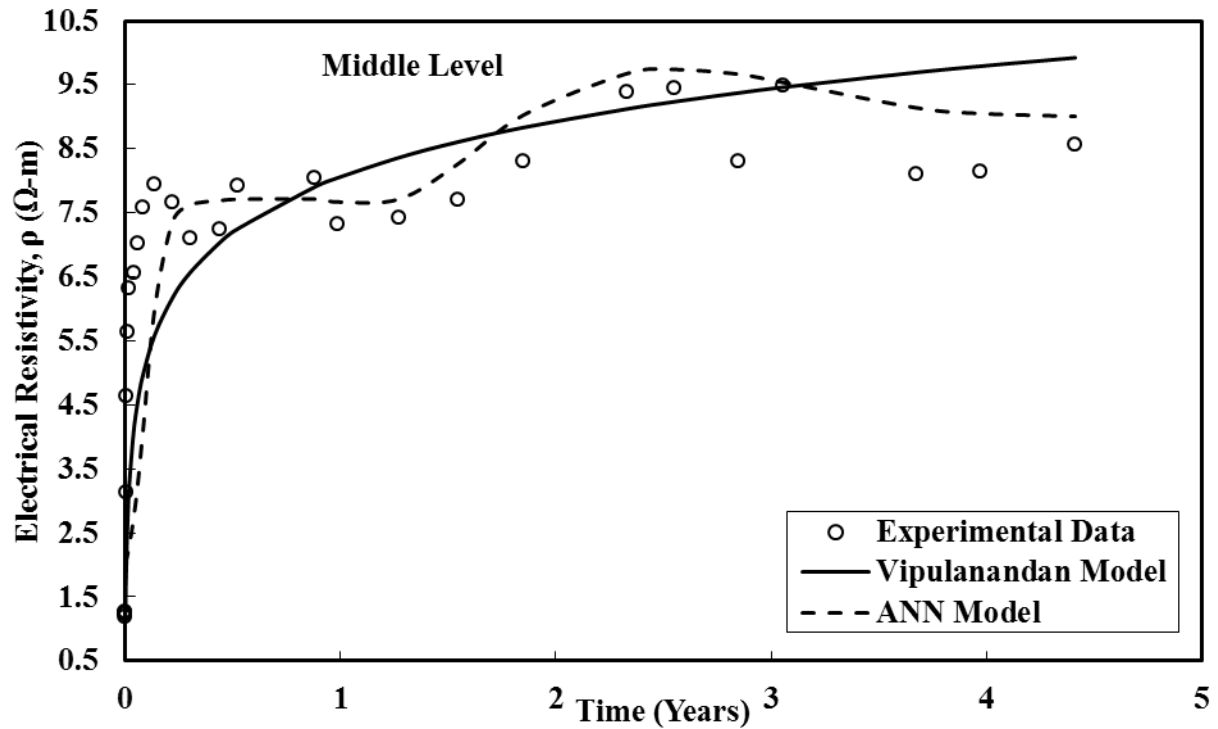


Figure 14. Comparing the Prediction of Electrical Resistivity at the Middle Level Using the AI Model and Vipulanandan Curing Model up to 4.5 years.

Bottom Level

The value of initial resistivity of smart cement was 1.32 Ω.m immediately after mixing. The electrical resistivity of smart cement was 4.91 Ω.m. after 4.5 years of curing (Figure 15). The time for minimum resistivity was 288 minutes after mixing (Table 5). Based on the preliminary analyses, AI model with for layers of ANN was selected predict the resistivity change with time. Over 30 data was used perform the BPNN and also predict the experimental trend. Curing Model parameters p_1 and q_1 were 0.84 and 0.15 respectively after 4.5 years of curing (Table 5). Also the other curing model parameters are summarized in Table 5. The value of RMSE (root mean square error) for electrical resistivity model was 0.25 Ω.m while it was 0.43 Ω.m for AI model. The value of R^2 for electrical resistivity model was 0.95 while it was 0.86 for AI model (Table 6). Thus, Vipulanandan curing model had comparatively better prediction for long term compared to the AI model.

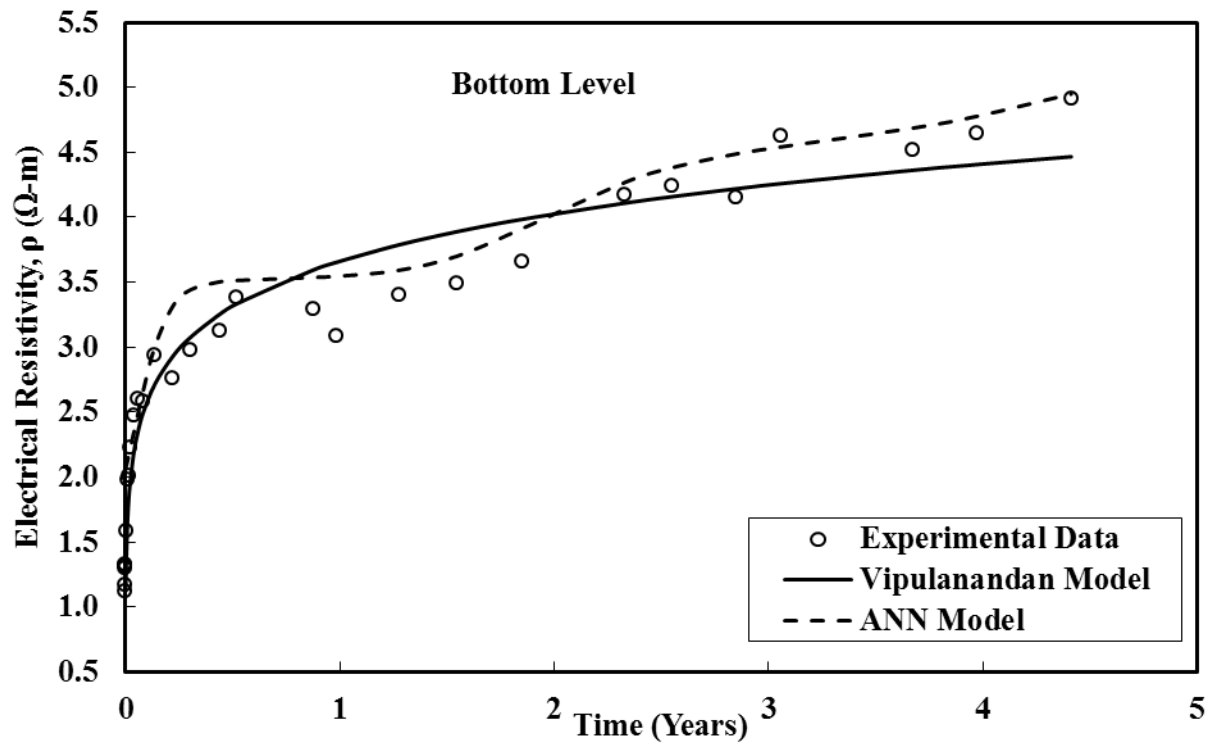


Figure 15. Comparing the Prediction of the Electrical Resistivity at the Bottom Level Using the AI Model and Vipulanandan Curing Model up to 4.5 years.

Table 5. Electrical resistivity model parameters for smart cement in field for 4.5 years.

	Curing Model				
Level	ρ_o ($\Omega.m.$)	t_{min} (min)	t_o (min)	p_1	q_1
Top	1.03	195	250	0.76	0.24
Middle	1.24	195	300	0.78	0.22
Bottom	1.32	288	136	0.84	0.15

Table 6. Correlation parameters for ANN Model and Resistivity model for smart cement in field after 4.5 years.

	ANN Model		Curing Model	
Level	R^2	RMSE	R^2	RMSE
Top	0.91	1.02	0.97	0.86
Middle	0.61	1.73	0.91	1.44
Bottom	0.86	0.43	0.95	0.25

Piezoresistivity Prediction

It is important to demonstrate the piezoresistivity of smart cement in the field. Also it is important to show the sensitivity of smart cement for small pressure changes. Hence the test was performed at 10 psi (0.07 MPa) increments up to 80 psi (0.55 MPa). The maximum value of piezoresistive strain for smart cement after 4.5 years of curing was 13.5% at a stress of 0.55 MPa (Figure 16). This is a clear demonstration of sensitivity of the smart cement. Also by measuring the piezoresistive strain in the smart cement it will be possible predict the pressure in the casing using the models. The value of model parameters p_2 and q_2 for piezoresistivity model are 0.025 and 0.417. AI model had a RMSE of 0.015 Ωm value compared to piezoresistivity model RMSE of 0.02 Ωm with a coefficient of determination of 0.99 (Table 7). Hence both models predicted the piezoresistive behavior of the smart cement.

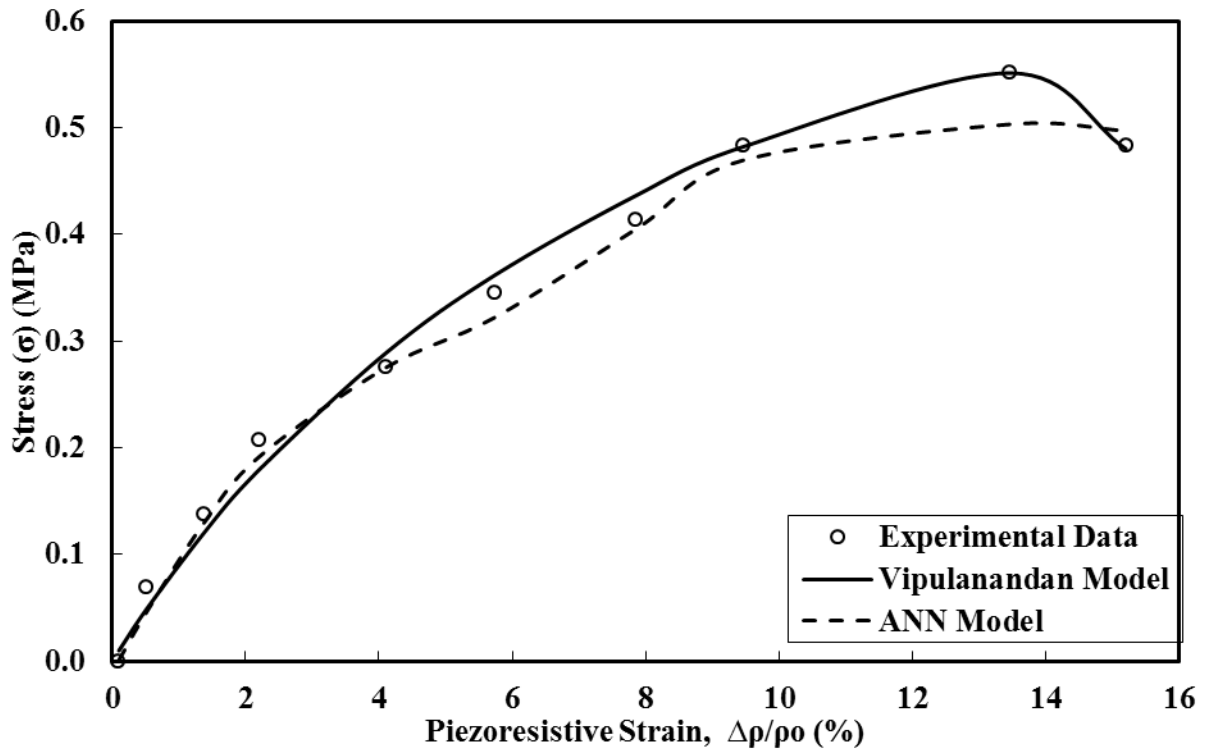


Figure 16. Piezoresistive Strain for smart cement in the field after 4.5 years of curing.

Table 7: Correlation parameters for ANN Model and piezoresistivity model for smart cement in field after 4.5 years.

Pressure Test on Smart Cement			
ANN Model		Piezoresistivity Model	
R^2	RMSE(Ωm)	R^2	RMSE (Ωm)
0.99	0.015	0.99	0.02

5. Conclusions

In this study Artificial Intelligent (AI) models were developed and used to predict behavior of smart cement and weather using the data collected from the laboratory tests and field tests and compared the predictions to the Vipulanandan Models. Over 1500 data were used in this study. Based on this study following conclusions are advanced:

1. AI models with one, two, three and four layers of artificial neural networks were evaluated using the laboratory and field data with the statistical parameter coefficient of determination (R^2) and root mean square error (RMSE). Based on the type of available data both Generalized Regression Neural Networks (GRNN) and Back Propagation Neural Network (BPNN) were used to train the AI models.
2. Based on the laboratory data and field data, electrical resistivity showed the largest variation compared to strain and temperature changes. Hence electrical resistivity was selected as the monitoring parameter for the smart cement.
3. AI model predicted the long-term smart cement curing with the resistivity parameter very well and was comparable to the Vipulanandan Curing Model. AI model did not predict the short-term curing well compared to the Vipulanandan Curing Model.
4. AI model predicted the smart cement piezoresistive behavior in the laboratory and field very well. Vipulanandan p-q piezoresistive model predicted the behavior well.
5. There is a need to further improve the AI predictions of resistivity change in the field. Vipulanandan curing model predicted the behavior very well.

6. Acknowledgements

This study was supported by the Department of Energy (DOE/NETL/RPSEA), National Science Foundation (NSF-I Corp), the Center for Innovative Grouting Materials and Technology (CIGMAT) and the Texas Hurricane Center for Innovative Technology (THC-IT) at the University of Houston, Texas. Sponsors are not responsible for the entire conclusion made from this study.

7. References

1. Alexander, I., and Morton, H. (1990). An Introduction to Neural Computing, 1th Ed., Chapman & Hall, Inc., pp. X-XV, Padstow, Cornwall.
2. Altunkaynak, A. (2007). "Forecasting Surface Water Level Fluctuations of Lake Van by Artificial Neural Networks." Water Resources Management, 21, 399-408.
3. Armour, T., Groneck, P., Keeley, J. and Sharma, S. (2000). "Micropile Design and Construction Guidelines Implementation Manual," FHWA-SA-97-070.
4. Bhattacharyya, P. (2011) "Neural Networks: Evolution, Topologies, Learning Algorithms and Applications". IGI Global Publisher.
5. Choolaei, M., Rashidi, A. M., Ardjmand, M., Yadegari, A. and Soltanian, H. (2012). The effect of nanosilica on the physical properties of oil well cement. Materials Science and Engineering: A, 538, 288-294.
6. Demircan, E., Harendra, S. and Vipulanandan, C.(2011) "Artificial Neural Network and Nonlinear Models for Gelling Time and maximum Curing

- Temperature Rise in Polymer Grouts,” *Journal of Materials in Civil Engineering*, Vol. 23, No. 4 , pp. 1-6, 2011.
7. Hammoudi, A., Moussaceb, K., Belebchouche, C. and Dahmoune, F. (2019) “Comparison of artificial neural network (ANN) and response surface methodology (RSM) prediction in compressive strength of recycled concrete aggregates”. *Construction and Building Materials*, 2019.
 8. Han, B., Guan, X. and Ou, J. (2007). Electrode design, measuring method and data acquisition system of carbon fiber cement paste piezoresistive sensors. *Sensors and Actuators A: Physical*, 135(2), 360-369.
 9. Han, B., Zhang, L. Zhang, C., Wang, Y., Yu, X. and Ou, J. (2016). Reinforcement Effect and mechanism of Carbon Fibers to Mechanical and Electrically Conductive Properties of Cement-Based Materials, *Construction and Building materials*, Vol. 125, pp. 479-489.
 10. Houk, A. N. *Self-Sensing Cementitious Materials*. (PhD dissertation), University of Kentucky, 2017.
 11. Hou, P., Qian, J., Cheng, X. and Shah, S. P. (2015). Effects of the pozzolanic reactivity of nanoSiO₂ on cement-based materials. *Cement and Concrete Composites*, 55, 250-258.
 12. Labibzadeh, M., Zahabizadeh, B. and Khajehdezfuly, A. (2010). Early-age compressive strength assessment of oil well class G cement due to borehole pressure and temperature changes. *Journal of American Science*, 6(7), 1-7.
 13. Mangadlao, J. D., Cao, P. and Advincula, R. C. (2015). Smart cements and cement additives for oil and gas operations. *Journal of Petroleum Science and Engineering*, 129, 63-76.
 14. McCarter, W. J., Starrs, G. and Chrisp, T. M. (2000). Electrical conductivity, diffusion, and permeability of Portland cement-based mortars. *Cement and Concrete Research*, 30(9), 1395-1400.
 15. McCarter, W. J., Chrisp, T. M., Starrs, G. and Blewett, J. (2003). Characterization and monitoring of cement-based systems using intrinsic electrical property measurements. *Cement and Concrete Research*, 33(2), 197-206.
 16. McCarter, W. J. (1994). A parametric study of the impedance characteristics of cement-aggregate systems during early hydration. *Cement and concrete research*, 24(6), 1097-1110.
 17. Mohammed, A. S. (2017). Electrical resistivity and rheological properties of sensing bentonite drilling muds modified with lightweight polymer. *Egyptian Journal of Petroleum*, 10.1016/j.ejpe.2017.10.018.
 18. Mohammed, A. (2017) . Vipulanandan model for the rheological properties with ultimate shear stress of oil well cement modified with nanoclay, DOI 10.1016/j.ejpe.2017.05.007.
 19. Opeyemi, B., Catalin, T. and Tanveer, Y. (2016) “Application of Artificial Intelligence Techniques in Drilling System Design and Operations: A State of the Art Review and Future Research Pathways”. *SPE Nigeria Annual International Conference and Exhibition*, August 2016.

20. Polder, R. B. (2001). Test methods for on-site measurement of resistivity of concrete—a RILEM TC-154 technical recommendation. *Construction and building materials*, 15(2), 125-131.
21. Rogers, M. J., Dillenbeck, R. L. and Eid, R. N. (2004). Transition Time of Cement Slurries, Definitions and Misconceptions, Related to Annular Fluid Migration. SPE Annual Technical Conference and Exhibition. <https://doi.org/10.2118/90829-MS>.
22. Rosenblatt, F. (1962). *Principles of Neurodynamics: Perceptrons and the Theory of Brain Mechanisms*, Spartan Books, New York.
23. Sadiq, T. and Nashawi, I. S. (2000) “Using Neural Networks for Prediction of Formation Fracture Gradient”, SPE/PS-CIM International Conference on Horizontal Well Technology, 2000.
24. Saridemir, M. (2009). “Prediction of Compressive Strength of Concretes Containing Metakolin and Silica Fume by Artificial Neural Networks.” *Advances in Engineering Software*, 40, 350-355.
25. Shadravan, A. and Amani, M. (2012). HPHT 101-what petroleum engineers and geoscientists should know about high pressure high temperature wells environment. *Energy Science and Technology*, 4(2), 36-60.
26. Shahab, D. (2000) “Virtual-Intelligence Applications in Petroleum Engineering: Part 1-Artificial Neural Networks”. SPE 58046-JPT, 2000.
27. Vipulanandan, C. and Paul, E. (1990). Performance of epoxy and polyester polymer concrete. *Materials Journal*, 87(3), 241-251.
28. Vipulanandan, C. and Krishnan, S., (1993) "XRD Analysis and Leachability of Solidified Phenol-Cement Mixtures," *Cement and Concrete Research*, Vol. 23, pp. 792-802.
29. Vipulanandan, C. and Sett, K. (2004). Development and characterization of piezoresistive smart structural materials. In *Proceedings of the Ninth Biennial ASCE Aerospace Division International Conference on Engineering, Construction, and Operations in Challenging Environments* (pp. 656-663).
30. Vipulanandan, C. and Garas, V. (2008). Electrical resistivity, pulse velocity, and compressive properties of carbon fiber-reinforced cement mortar. *Journal of Materials in Civil Engineering*, 20(2), 93-101.
31. Vipulanandan, C. and Prashanth, P. (2013). Impedance spectroscopy characterization of a piezoresistive structural polymer composite bulk sensor. *Journal of Testing and Evaluation*, 41(6), 1-7.
32. Vipulanandan, C., Ali, K., Basirat, B., A. Reddy, Amani, N., Mohammed, A. Dighe, S., Farzam, H. and W. J. Head (2016), “Field Test for Real Time Monitoring of Piezoresistive Smart Cement to Verify the Cementing Operations ,” OTC-27060-MS.
33. Vipulanandan, C. and Mohammed, A. S. (2014). Hyperbolic rheological model with shear stress limit for acrylamide polymer modified bentonite drilling muds. *Journal of Petroleum Science and Engineering*, 122, 38-47.
34. Vipulanandan, C. and Mohammed, A. (2015). Smart cement rheological and piezoresistive behavior for oil well applications. *Journal of Petroleum Science and Engineering*, 135, 50-58.
35. Vipulanandan, C., Krishnamoorti, R., Mohammed, A., Boncan, V., Narvaez, G., Head, B. and Pappas, J. M. (2015). Iron Nanoparticle Modified Smart Cement

- for Real Time Monitoring of Ultra Deepwater Oil Well Cementing Applications, OTC-25842-MS.
36. Vipulanandan, C. and Mohammed, A. (2015). Smart cement modified with iron oxide nanoparticles to enhance the piezoresistive behavior and compressive strength for oil well applications. *Smart Materials and Structures*, 24(12), 125020.
 37. Vipulanandan, C. and Mohammed, A. (2017). Rheological Properties of Piezoresistive Smart Cement Slurry Modified With Iron-Oxide Nanoparticles for Oil-Well Applications. *Journal of Testing and Evaluation*, 45(6).
 38. Vipulanandan, C. and Mohammed, A. (2015). XRD and TGA, Swelling and Compacted Properties of Polymer Treated Sulfate Contaminated CL Soil. *Journal of Testing and Evaluation*, 44(6).
 39. Vipulanandan, C., and Mohammed, A. (2015). Effect of nanoclay on the electrical resistivity and rheological properties of smart and sensing bentonite drilling muds. *Journal of Petroleum Science and Engineering*, 130, 86-95.
 40. Vipulanandan, C., Ali, M., Basirat, B., Reddy, A., Amin, N., Mohammed, A., & Farzam, H. (2016). Field Test for Real Time Monitoring of Piezoresistive Smart Cement to Verify the Cementing Operations. In *Offshore Technology Conference*. Offshore Technology Conference.
 41. Vipulanandan, C., Mohammed, A., and Samuel, R. G. (2017). Smart Bentonite Drilling Mud Modified with Iron Oxide Nanoparticles and Characterized Based on the Electrical Resistivity and Rheological Properties with Varying Magnetic Field Strengths and Temperatures. In *Offshore Technology Conference*. Offshore Technology Conference.
 42. Vipulanandan, C., and Mohammed, A., (2017) "Rheological Properties of Piezoresistive Smart Cement Slurry Modified With Iron Oxide Nanoparticles for Oil Well Applications." *Journal of Testing and Evaluation*, ASTM, Vol. 45 Number 6, pp. 2050-2060.
 43. Vipulanandan, C., and Ali, K., (2018) "Smart Cement Grouts for Repairing Damaged Piezoresistive Cement and the Performances Predicted Using Vipulanandan Models" *Journal of Civil Engineering Materials*, American Society of Civil Engineers (ASCE), Vol. 30, No. 10, Article number 04018253.
 44. Vipulanandan, C., and Amani, N., (2018) "Characterizing the Pulse Velocity and Electrical resistivity Changes In Concrete with Piezoresistive Smart Cement Binder Using Vipulanandan Models" *Construction and Building Materials*, Vol. 175, pp. 519-530.
 45. Vipulanandan, C., and Mohammed, A., (2018) "Smart Cement Compressive Piezoresistive Stress-Strain and Strength Behavior with Nano Silica Modification," *Journal of Testing and Evaluation*, ASTM, doi 10.1520/JTE 20170105.
 46. Vipulanandan, C., G. Panda, G., Maddi, A.R., Wong, G. and Aldughather, A. (2019) "Characterizing Smart Cement Modified with Styrene Butadiene Polymer for Quality Control, Curing and to Control and Detect Fluid Loss and Gas Leaks Using Vipulanandan Models," *Offshore Technology Conference (OTC) 2019*, OTC-29581-MS, (OTC-2019), CD Proceeding, Houston, Texas, May 2019.

47. Wei, X., Xiao, L. and Li, Z. (2012). Prediction of standard compressive strength of cement by the electrical resistivity measurement. *Construction and Building Materials*, 31, 341-346.
48. Xiao, L. and Li, Z. (2008). Early-age hydration of fresh concrete monitored by non-contact electrical resistivity measurement. *Cement and Concrete Research*, 38(3), 312-319.